RESEARCH ARTICLE

VOLCANICA

Halogen (Cl, F) and sulphur release during explosive, effusive, and intrusive phases of the 2011 rhyolitic eruption at Cordón Caulle volcano (Chile)

C. Ian Schipper*[α], Jonathan M. Castro[β], Ben M. Kennedy[γ], Bruce W. Christenson[δ], Alessandro Aiuppa[ϵ], Brent Alloway[ζ, η], Pablo Forte[β], Gilles Seropian[γ], Hugh Tuffen[θ]

[α] *School of Geography, Environment and Earth Sciences, Victoria University, PO Box 600, Wellington 6140, New Zealand.*
[β] *Institute of Geosciences, University of Mainz, Mainz, Germany.*
[γ] *Geological Sciences, University of Canterbury, Christchurch, New Zealand.*
[δ] *National Isotope Centre, GNS Science, PO Box 31-312, Lower Hutt 5040, New Zealand.*
[ϵ] *Dipartimento DiSTeM, Università di Palermo.*
[ζ] *School of Environment, The University of Auckland, Private Bag 92019, Auckland, New Zealand.*
[η] *Instituto de Geografía, Pontificia Universidad Catolica de Chile, Av. Vicuna Mackenna, 4860, Santiago, Chile.*
[θ] *Lancaster Environment Centre, Lancaster University, LA1 4YQ, UK.*

Abstract

We investigate sulphur, chlorine and fluorine release during explosive, effusive and intrusive phases the 2011-2012 Cordón Caulle eruption, with a focus on the halogens. Analysis of melt inclusions, pyroclasts and lava samples shows most sulphur to have degassed during magma decompression, but halogen release to have accompanied isobaric crystallisation in slowly-cooled magma that was emplaced in a lava flow and sub-vent intrusion. Fluorine in particular mobilised only after extensive groundmass crystallisation and incipient devitrification. By 2017, gas emitted from vent-proximal fumaroles had hydrothermal compositions, with HCl/HF ratios correlating with temperature. We estimate that the eruption could eventually emit up to 0.92 Mt of SO_2, 6.3 Mt of HCl, and 1.9 Mt of HF, but only ~16 wt.%, ~7 wt.% and ~2 wt.% of these were respectively emitted during opening explosive phases. Halogen devolatilisation and its associated hazards can persist long after rhyolite eruption and/or emplacement.

Keywords: Puyehue-Cordón Caulle; Halogens; Rhyolite; Volatile Budget; Lava Flow

1 Halogens in volcanic systems

Nearly all aspects of volcanism are controlled by volatiles (H_2O, CO_2, S, Cl, F), which play different roles at different times in the lifetime of a magma body [e.g. Westrich et al. 1988; Carroll 1994; Sparks 2003; Cashman 2004; Edmonds and Wallace 2017]. Among these major volatiles, the halogens chlorine and fluorine are the most poorly understood [e.g. Aiuppa et al. 2009; Webster et al. 2018]. Their release from ascending magma is not a simple consequence of decompression, and conditions of magma emplacement are important in controlling if and how they become mobile [Kilinc and Burnham 1972; Villemant and Boudon 1999; Edmonds et al. 2002]. Although they do not drive eruptions [e.g. like H_2O and CO_2: Cashman 2004], or provide easily-measured proxies for magmatic vitality [e.g. like sulphur species: Giggenbach 1996; Symonds et al. 2001], they can significantly influence melt properties [e.g. Dingwell and Hess 1998], are highly reactive in volcanic edifices and plumes [Symonds et al. 1987; Wolff-Boenisch et al. 2004; Bellomo et al. 2007], play a key role in the genesis of economically important mineral resources [McPhie et al. 2011], and can have detrimental effects on the environment, the atmosphere, animals and people [Cronin et al. 2003; Delmelle 2003; D'Alessandro 2006; von Glasow et al. 2009; Flueck and Smith-Flueck 2013].

Methods for quantifying chlorine and fluorine species in volcanic rocks and gases are improving [e.g. Waters et al. 2006; Zhang et al. 2016; Roberts et al. 2017] and catalogues of halogen concentrations in volcanic gases are growing [Pyle and Mather 2009; Webster et al. 2018]. Still, there is little information on the behaviour of these halogens during rhyolite eruptions [Shinohara et al. 1993; Mori et al. 2002; Lowenstern et al. 2012]. This is partly because there have been so few historical eruptions of silicic magma, and is problematic because halogens can become highly concentrated in evolved melts [Carroll 1994], and because silicic eruptions tend to be highly explosive and have

*Corresponding author: ian.schipper@vuw.ac.nz

widespread effects. Here, we examine the release of chlorine and fluorine, and also sulphur, during different phases of the 2011–2012 rhyolite eruption at Cordón Caulle volcano (Chile), in order to establish the degree and timing of halogen output during explosive, effusive, and intrusive rhyolite volcanism.

A weakly inverse relationship between chlorine solubility and pressure in metaluminous rhyolites means Cl does not spontaneously degas during magma ascent [Metrich and Rutherford 1992]. Rather, it tends to partition into the aqueous fluids generated by decompression-driven exsolution of magmatic H_2O [Kilinc and Burnham 1972]. Affinity for the fluid phase is described by the fluid-melt partitioning coefficient $D_{Cl}^{v/m} = [Cl]^v/[Cl]^m$, where [Cl] is chlorine concentration in aqueous vapour (v) and melt (m). In silicic melts, $D_{Cl}^{v/m}$ is most often in the range of 10–100, depending on melt composition and fluid availability [Baker and Alletti 2012, and references therein]. Chlorine diffusion is slow in silicic melts, and its exsolution is kinetically limited during rapid magma ascent [Baker and Balcone-Boissard 2009]. The most prodigious release of Cl is from magma that cools slowly in lava flows, domes, or shallow intrusions, where higher $D_{Cl}^{v/m}$ result from Cl being incompatibly concentrated in residual melts, where there is time for Cl diffusion out of melt, and where second boiling and hydrothermal circulation provide fluids into which Cl can partition [Westrich et al. 1988; Villemant and Boudon 1999; Harford et al. 2003; Villemant et al. 2008; Balcone-Boissard et al. 2010; Lowenstern et al. 2012; Bégué et al. 2017]. The importance of slow isobaric crystallisation to Cl release manifests during eruptions as HCl emissions being weaker during explosive phases and stronger during effusive phases of chemically equivalent magma [Edmonds et al. 2002].

The mechanisms of fluorine degassing are insufficiently explained and appear paradoxical. Fluorine is highly soluble in silicate melts [Carroll 1994], and can be present to weight per cent levels in highly-evolved magmas [e.g. Webster 1990]. It also has a strong affinity for melts over aqueous fluids, with $D_F^{v/m}$ usually being <1, although $D_F^{v/m}$>10 have been experimentally determined for mafic systems [Baker and Alletti 2012, and references therein]. Fluorine should therefore be expected to behave incompatibly during crystallisation of volatile-free mineral assemblages [Aiuppa et al. 2009; Balcone-Boissard et al. 2010]. However, there is ample evidence for significant fluorine degassing and/or mobilisation during volcanic eruptions. Direct evidence is in the measurable fluorine in volcanic plumes [Bellomo et al. 2007; Aiuppa et al. 2009; Pyle and Mather 2009]. This is usually as HF, although SiF_4 has also been measured in plumes from arc rhyolites [Mori et al. 2002]. Fluorine is also a ubiquitous and hazardous component of leachates from fresh ash [Cronin et al. 2003; Stewart et al. 2016]. Indirect evidence for fluorine degassing is in the inferred role of HF in corroding volcanic glass and redistributing SiO_2 via SiF_4, depositing it as metastable silica polymorphs (cristobalite) in pore spaces [Wolff-Boenisch et al. 2004; de Hoog et al. 2005; Horwell et al. 2013; Schipper et al. 2017]. Our understanding of fluorine behaviour is partly hindered by its reactivity with aluminosilicate materials [Cronin et al. 2003; Wolff-Boenisch et al. 2004; Delmelle et al. 2007], its tendency to be scrubbed from volcanic gases [Symonds et al. 2001], and the solubility of its various salts and compounds in water [Cronin et al. 2003; D'Alessandro 2006; Wardell et al. 2008].

We investigate the behaviour of chlorine and fluorine at Cordón Caulle volcano (Chile, Figure 1), and include a comparative assessment to sulphur release. This is achieved using a combined textural and petrological approach augmented with a few measurements of post-eruptive fumarolic gas compositions. This VEI 5 eruption is the largest 21st century subaerial eruption to-date, and is only the second eruption of rhyolite magma to have been closely observed, after Chaitén in 2008–2009 [e.g. Lowenstern et al. 2012]. During the paroxysmal phase of this eruption three distinct but cogenetic magma bodies were simultaneously tapped [Alloway et al. 2015].

The 2011–2012 Cordón Caulle eruption is ideal for investigating halogen mobility because it included several distinctly different phases, from an early Plinian phase, through prolonged simultaneous explosive/effusive activity, to a protracted period of endogenous lava advance [Castro et al. 2013; Schipper et al. 2013; Tuffen et al. 2013] (Figures 1 and 2A). Additionally, there was a shallow, large-volume magmatic intrusion emplaced in the first month of the eruption [Castro et al. 2016]. Extrusive products experienced a wide range of emplacement and cooling histories, and have correspondingly diverse textural characteristics [Schipper et al. 2015; Magnall et al. 2018] and intrusion of the laccolith [Castro et al. 2016] caused significant uplift in the vent region accompanied by elevated heat and gas fluxes at the surface (Figures 1 and 2B). This diversity of magma emplacement regimes provides an opportunity to investigate halogen behaviour during various permutations of rhyolite volcanism.

1.1 Cordón Caulle volcano and the sampled eruption products

The Cordón Caulle fissure system is the site of the three most recent eruptions, in 1921, 1960, and 2011, from the Puyehue–Cordón Caulle Volcanic Complex (PCCVC) in the Southern Volcanic Zone of the Chilean Andes (Figure 1). This volcanic complex has been active since the Pleistocene and has erupted a wide range of magma types. Background to the PCCVC and recent activity at Cordón Caulle can be found in Gerlach et al. [1988], Lara et al. [2006], and Singer et al. [2008].

The samples analysed in this work were collected

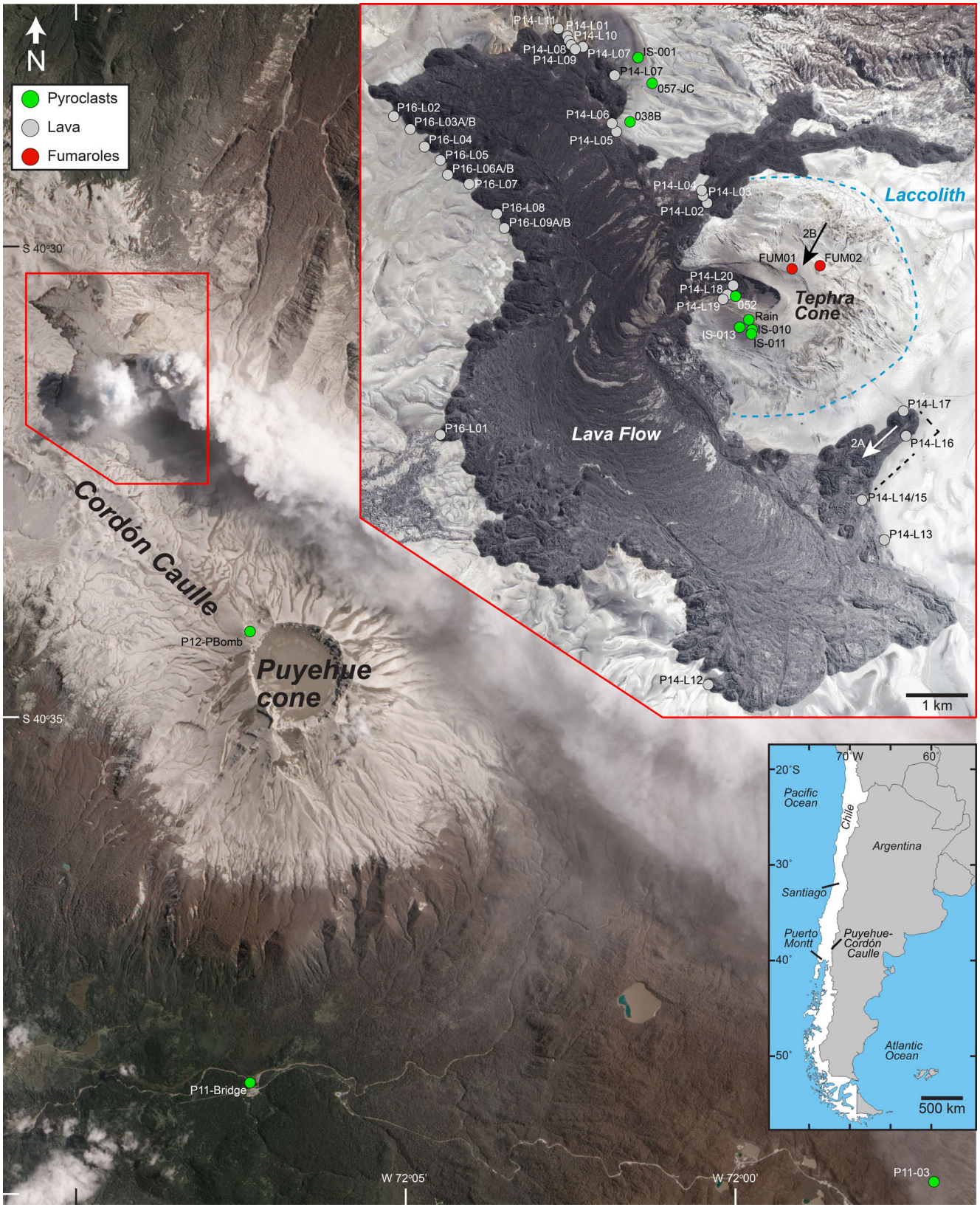

Figure 1: Location and samples. Main image was taken by the Advanced Land Imager on NASA's Earth Observing-1 (EO-1) satellite on January 26, 2012. Inset of 2011–2012 eruptive features and deposits is from Google (2017, DigitalGlobe), with approximate extent of the laccolith indicated by blue dashed line [Castro et al. 2016]. Arrows indicate view directions shown in Figure 2. Inset map shows location of Puyehue–Cordón Caulle in southern Chile.

during several field campaigns from 2011–2017. Pyroclastic samples include pumice from Plinian deposits up to 24 km from the vent, and obsidian bombs ejected to ≤1.6 km from the vent by Vulcanian blasts that occurred during simultaneous explosive/effusive activity (Figure 1).

The majority of our samples are from the extensive 2011–2012 Cordón Caulle lava flow (Figure 1). This flow continued to advance by endogenous processes for more than one year after the delivery of new magma to the surface had ceased [Tuffen et al. 2013]. The main mechanism for this was by "breakouts" from stalled flow margins (Figure 2A), a process phenomenologically similar to that seen in advancing basaltic lavas, and one that has been the subject of several studies at Cordón Caulle [Tuffen et al. 2013; Farquharson et al. 2015; Magnall et al. 2017; Magnall et al. 2018]. Our lava samples (n = 32) were mostly obtained from these breakouts (Figure 1). This sampling strategy was partly designed to capture the textural evolution associated with lava advance and emplacement [Magnall et al. 2018], but was also dictated by practicality. The lava flow is unstable, with margins several tens of metres high that made it difficult and unsafe to physically access the flow interior, except in a few places (Figure 2A). Consequently, the suite of lava samples robustly catalogues the range of textures found in the flow, but over-represents its overall glass content, as breakouts and flow surfaces tend to be partially glassy (see Figures 4 and 5), but the majority of the flow volume consists of dense holocrystalline material [Schipper et al. 2015; Magnall et al. 2018]. Figure 2A shows an aerial view of a rifted breakout, which has a partially glassy, but thin (~1 m) upper surface, and a dense holocrystalline interior. We obtained only a few samples that are representative of this dense flow core (see Figure 4, sample P14-L05), but observations in the field and by aerial photogrammetry [Schipper et al. (unpublished data)]; Figure 2A] suggest these to be most representative of the flow as a whole.

2 Analytical methods

Polished thin sections of all samples were scanned using transmitted light on a flatbed scanner. Groundmass textures were examined using backscatter electron (BSE) imaging on a JEOL JXA-8230 Superprobe at Victoria University of Wellington (VUW). For each sample, a series of five representative BSE images were collected at 250× magnification, with brightness and contrast optimised to allow segmentation of different groundmass phases. The proportions of glass, plagioclase, pyroxene, Fe-Ti oxides, and SiO_2 were quantified by manually thresholding and calculating the area fraction of each phase in each image, using ImageJ [Schneider et al. 2012].

A suite of representative samples covering the different phases of the eruption were powdered in a tungsten-carbide mill and fused into glass beads. Major elements were determined by X-Ray Fluorescence (XRF) using a Phillips MagiXPRO instrument at the University of Mainz.

Major element compositions of minerals and glasses, and volatile (S, Cl, F) contents of glasses were determined by electron probe microanalysis (EPMA), with the JEOL JXA-8230 at VUW. In phenocrysts and microlites, major elements were determined using an accelerating voltage of 15 kV, current of 12 nA, peak/background count times of 30 s/15 s, and a focused beam, standardised against plagioclase (NMNH 115900), Kakanui augite (USNM 122142), and synthetic oxides [Jarosewich et al. 1980]. In melt inclusions and matrix glasses, major elements were determined using 15 kV, 8.0 nA, peak/background count times of 30 s/15 s, and a beam defocused to 10 µm, where possible. In order to minimise sodium volatilisation during analysis of glasses, Na was measured first, for shorter times (10 s/5 s), and at a fixed peak position in order to eliminate the need for a peak search procedure. Major element analyses were standardised using natural and synthetic compounds [Jarosewich et al. 1980] as follows: basaltic glass standard VGA-99 for Ca, Mg, Fe; rhyolitic glass standard VG-568 for Si, Al, Na, K; synthetic oxides for Ti, Mn, Cr. In highly crystalline lava samples, regions of residual glass were too small to accommodate a 10 µm beam. On these, the beam size was reduced to as low as 1 µm, but regular checking of secondary standards did not indicate any significant volatilisation of Na even when spot analyses were used (Figure 3A).

Volatile analyses were performed in a second run that utilised the same pre-programmed analytical spots as used for major element analysis [e.g. Lowenstern et al. 2012], with accelerating voltage of 15 kV, current of 60 nA. Sulphur and chlorine were analysed for 60 s/30 s on peak/background. Sulphur was standardised against Elba Pyrite. Although the S-Kα peak position is a function of oxidation state, a narrow-band peak search in advance of each S-Kα measurement ensured that sample-specific peak positions were measured on each analytical spot. Chlorine was standardised against VG-568, and was analysed simultaneously on two channels (with PETL and PETJ crystals). Detection limits for sulphur and chlorine were ~9 ppm and ~19 ppm, respectively. Fluorine was measured for 120 s/60 s on a W-Si multilayered pseudocrystal (LDE1). To eliminate interference between the F-Kα and Mg-Kβ peaks, we used pulse height analysis (PHA) settings described by Witter and Kuehner [2004] for use on JEOL instruments. To accommodate overlap between the F-Kα peak and the shoulder of the Fe-Lα peak, we followed the method of Zhang et al. [2016], whereby we obtained a calibration curves of apparent F at given Fe, by analysing a suite of Fe-bearing, F-free synthetic glasses (generously provided by C. Zhang).

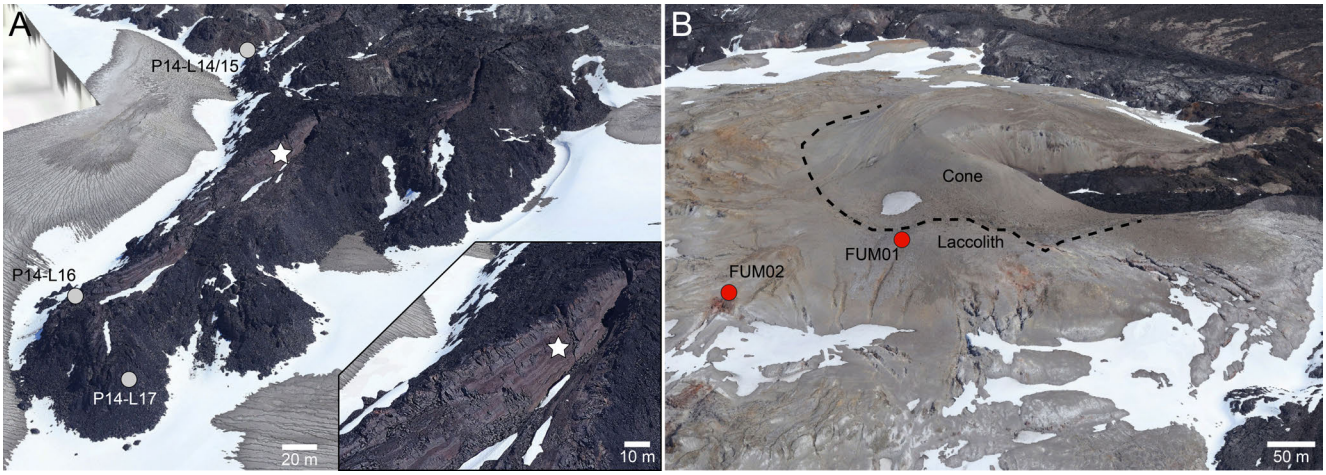

Figure 2: Key features of Cordón Caulle deposits. Images are from an aerial photogrammetry survey conducted in November 2017 [Schipper et al. (unpublished data)], corresponding to arrows marked in Figure 1. [A] Example breakout. Inset shows fracture that reveals internal textures of breakout material, indicating that the partially glassy upper surface is thin and that the majority of the flow is dense, holocrystalline material. [B] Overview of the 2011 vent, sitting atop the bulge created by syneruptive laccolith emplacement, and the locations of the fumaroles from which gases were analysed.

The detection limit for F was calculated to be 100–120 ppm, based on the standard deviation of analyses on Fe-bearing, F-free calibration glasses [following Zhang et al. 2016]. Measured concentrations of S, Cl, and F were routinely checked against a suite of secondary standard reference glasses, both natural [Indian Ocean Glass, VG-2, VGA-99, VG-568: Jarosewich et al. 1980; Jochum et al. 2005], and synthetic [AC-E, DR-N, GS-E: Zhang et al. 2016, Figure 3B–D].

The compositions of gases discharged from active fumaroles on the Cordón Caulle edifice were analysed in December 2017. The temperatures of several fumaroles were determined by a handheld, 1-metre-long K-type thermocouple. Concentrations of major gas species discharged from fumaroles were investigated using a multicomponent gas analyser system [MultiGAS: Aiuppa 2005; Shinohara 2005] built and calibrated at Palermo University (Italy). The MultiGAS system was equipped with sensors for CO_2, relative humidity, SO_2, H_2S, and H_2, recording at 1 Hz and a flow rate of ~1 L min^{-1}.

Concentrations of S, Cl, and F in fumarolic gases were determined by pumping gases at ~1 L min^{-1} through a glass bubbler apparatus filled with 4 molar NaOH solution. Bubblers were left in operation overnight in each fumarole. The concentrations of S (measured as SO_4 after oxidation of total S in the solution), Cl, and F in the resulting neutral solutions were determined by ion chromatography at the National Isotope Centre of the Institute of Geological and Nuclear Sciences in Lower Hutt using a DIONEX 3000 fitted with an AS19 column and using KOH as the eluant.

3 Results

3.1 Textures

The analysed pyroclasts range from high-porosity pumice produced during Plinian activity to high-

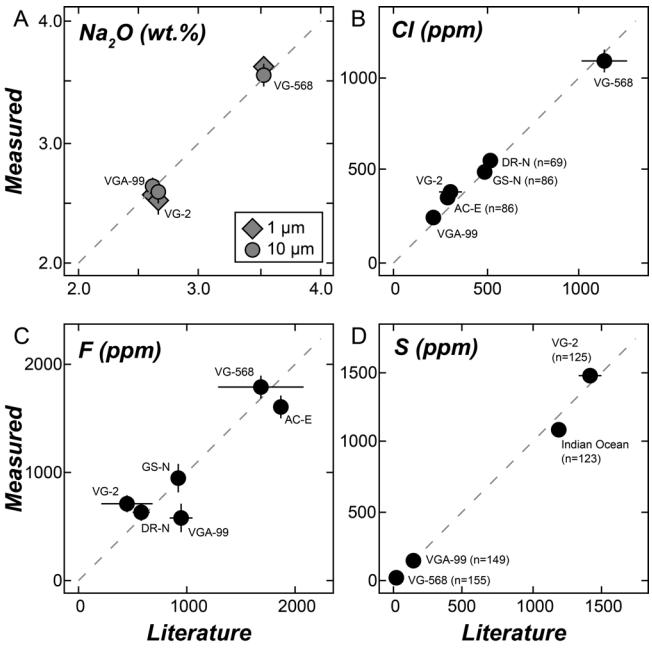

Figure 3: EPMA analysis of reference glasses. [A] Na_2O measured using 1 and 10 µm diameter electron beams. [B–D] Volatiles analysed using the method of Zhang et al. [2016]. Error bars are ±1 standard deviation and are often smaller than symbol sizes.

density obsidian produced during Vulcanian blasts (Figure 4A). Lava samples have porosities ranging from zero to 48 % (all textural features were measured as area %, but are assumed to represent vol.%). Texturally, the lava samples define a continuum or maturation sequence of progressive vesicle flattening sub-parallel to co-developing microlite-rich flow bands. At one end of this continuum are samples with sub-spherical vesicles set in a glassy groundmass (e.g. Figure 4B; P14-L06). Samples with intermediate textures have some flow banding and collapsed vesicles, as well as outsized vesicles (e.g. Figure 4B; P14-L10) that have been previously interpreted as evidence of second boiling [Magnall et al. 2018]. Some samples are completely dense with holocrystalline groundmass throughout (e.g. Figure 4B; P14-L05). Pores in lava samples, but not in pyroclasts, often have corroded rims and host vapour-phase cristobalite crystals [Schipper et al. 2015; Magnall et al. 2018].

Phenocryst populations in all samples are similar to those reported by Castro et al. [2013]: ~5 % total, of plagioclase > 2-pyroxenes > Fe-Ti oxides +/− apatite, with crystals often found in polymineralic glomerocrysts. Apatite is the only observed volatile-bearing mineral, but is only an accessory phase (≪1 %). All of the analysed pyroclast matrix glasses are free of microlites (Figure 2A). Conversely, lava samples have groundmasses with microlite contents ranging from 28–90 % (Figure 4B, Figure 5A).

Within the microlite populations, proportions of Fe–Ti oxides (1.0 ± 0.5 %) and pyroxene (2.9 ± 0.8 %) do not vary systematically between lava samples, but the relative proportions of other groundmass phases change as total groundmass crystallinity increases (Figure 5A). From 28 to 55 % crystallinity, the abundance of plagioclase microlites (An_{17}–An_{35}; Figure 5B) increases steadily. Above 55 % crystallinity, there is a plateau in plagioclase abundance, and the proportion of crystalline SiO_2 in the groundmass starts to become significant, increasing sharply in samples with >63 % microlites. Above 75 % crystallinity, plagioclase abundance begins to increase again, and the proportion of crystalline SiO_2 continues to increase (Figure 5A). Previous work by laser Raman analysis on Cordón Caulle lava samples showed the crystalline SiO_2 to be metastable cristobalite, interpreted in this particular form to be the product of incipient groundmass devitrification [Schipper et al. 2015].

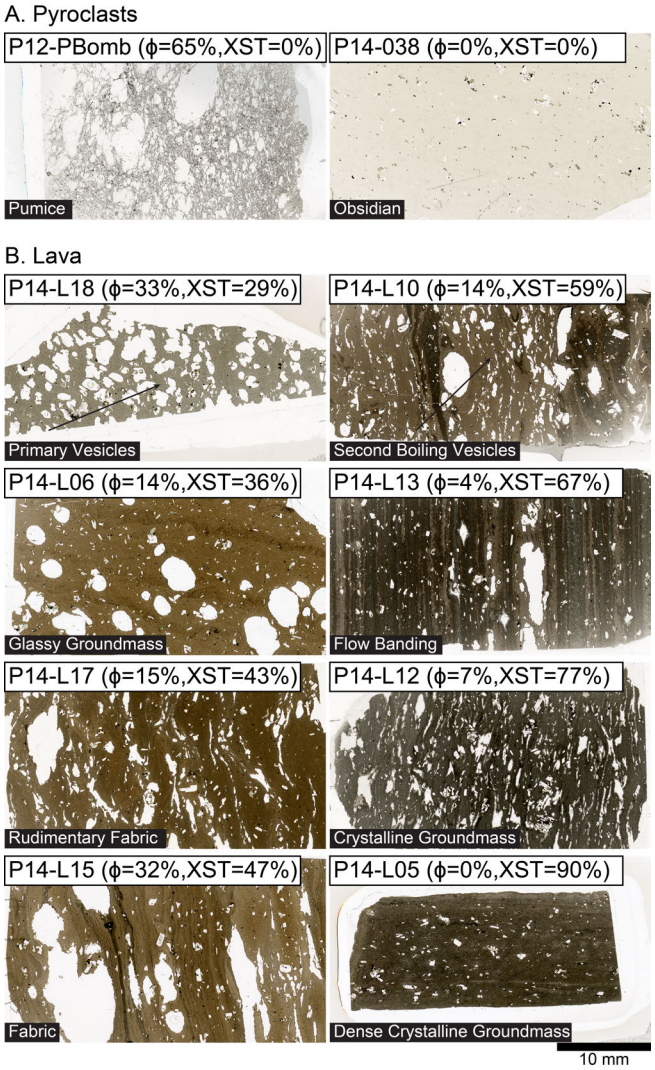

Figure 4: Thin sections of Cordón Caulle [A] pyroclasts and [B] lava samples, all at the same scale. Total porosity (ϕ) and groundmass crystallinity (XST) are shown as percentages, and key features are labelled. Lava samples document a progressive fabric development, with increased flattening of vesicles parallel to microlite-rich flow bands, until the material is avesicular and holocrystalline (in P14-L05). The dense sample P14-L05 is considered to be representative of the majority of the flow volume (e.g. inset to Figure 2A).

3.2 Major elements

Whole-rock analyses of pyroclasts (69.4–70.6 wt.% SiO_2) and lava (69.5–70.2 wt.% SiO_2) are indistinguishable in major elements (Figure 6A; Supplementary Data). Melt inclusions in plagioclase (An_{30}–An_{45}; Figure 5B) and pyroxene (Mg# 53–62; Figure 5C) partially overlap with whole-rock compositions, but also extend to as high as 72.7 wt.% SiO_2. Sample averages of pyroclast glasses range from 70.5–73.3 wt.% SiO_2, and define major element trends that are consistent with fractionation of the observed phenocryst assemblage. Lava matrix glasses are shown as sample averages in Figure 6, after individual spots with compositions indicative of contamination by plagioclase, pyroxene, or oxide crystals were rejected [Lowenstern et al. 2012]. Error bars show ±1 standard deviation, and indicate the degree of intra-sample compositional heterogeneity. Lava samples with ≤75 % groundmass crystallinity have SiO_2 ranging from 73.8–76.2 wt.% In this range, major element trends generally reflect progressive crys-

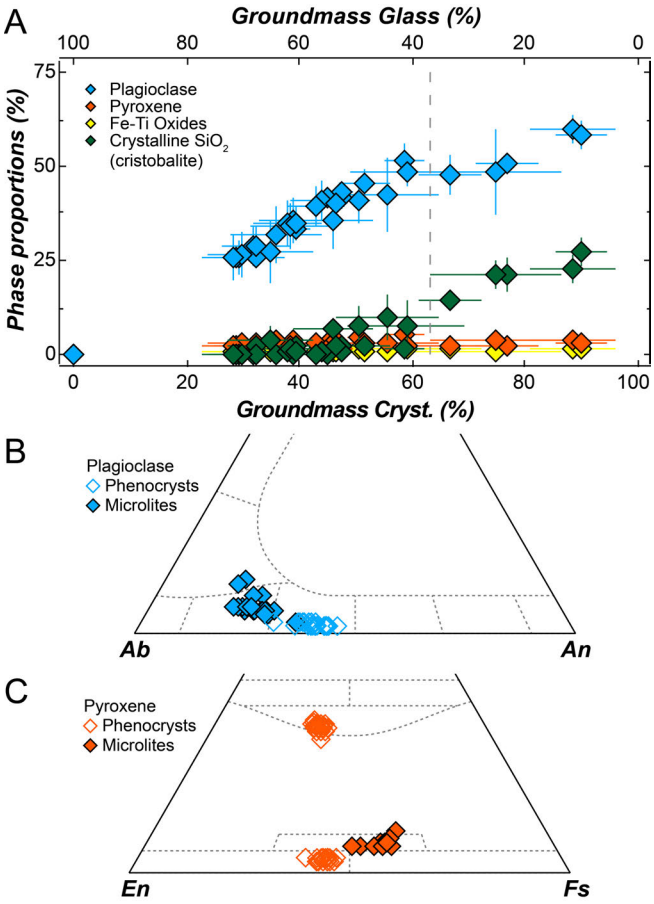

Figure 5: [A] Microlite abundances in each sample as a function of increasing total groundmass crystallinity (equivalent to declining groundmass glass). Crystalline SiO_2 becomes an important groundmass phase above ~63 % total crystallinity (vertical dashed line). Error bars are ± 1 standard deviation to proportions in multiple BSE images from each sample. [B–C] Compositions of plagioclase and pyroxene.

tallisation of the microlite assemblage (Figure 5), including plagioclase that is higher in K_2O ($Or_{7.0\pm2.4}$) than the phenocrysts ($Or_{2.0\pm0.3}$), and pyroxene that is exclusively pigeonite (Mg# 38–49), typical of orthopyroxene formed during quench crystallisation [Deer et al. 1992]. Except for a few outliers, lava matrix glasses generally define an increasing trend in TiO_2, indicating that although ilmenite is a phenocryst phase, the microlitic oxides are exclusively magnetite. Intra-sample variability in lava samples with ≤75 % microlites is relatively small but increases with sample crystallinity as the residual glass that was analysed was found in bands of high and variable crystallinity (e.g. sample P14-L13 in Figure 4B).

Major elements in the matrix glass of lava samples with >5 % microlites are off-trend from the rest of the suite and have SiO_2 ranging from 77.3–80.3 wt.%. The upper end of this range pushes the limit of silica content in pristine (e.g. non-devitrified) rhyolitic glasses formed at low pressures [e.g. Gualda and Ghiorso 2013]. This, and the observation that these samples contain groundmass cristobalite [Figure 5A; Schipper et al. 2015] suggests that these highly crystalline samples are starting to show compositional effects of devitrification [Lofgren 1970; Stix et al. 1995; Rowe et al. 2012]. The most notable changes with increasing groundmass crystallinity (and matrix glass SiO_2) are inflections in TiO_2, CaO, Na_2O and K_2O at >77 wt.% SiO_2 (or >5 % microlites; Figure 6A). Average compositions of matrix glasses in highly crystalline lava samples have large standard deviations, reflecting significant intra-sample heterogeneity in major elements (Figure 6A).

3.3 Volatiles

Figure 6B shows sulphur, chlorine, and fluorine concentrations versus SiO_2 in all melt inclusions and matrix glasses. Melt inclusions in plagioclase are generally lower in SiO_2 and higher in volatiles than those in pyroxene. The lowest-SiO_2 melt inclusion contains the maximum measured sulphur concentration (156 ppm) and S generally declines with increasing SiO_2. The maximum chlorine (2676 ppm) and fluorine (1365 ppm) concentrations are not in this same inclusion, and while Cl slightly increases with increasing SiO_2, F concentrations remain relatively constant, possibly influenced by the crystallisation of accessory (≪1 %) apatite. Two of the plagioclase-hosted melt inclusions have distinctly higher sulphur (149 ± 9 ppm) than the rest. These have average chlorine (2604 ± 25 ppm) and fluorine (1057 ± 436 ppm) values that are similar to the averages of the entire plagioclase-hosted melt inclusion suite (Cl = 2422 ± 202 ppm; F = 1026 ± 190 ppm). Sulphur concentrations are low in matrix glasses of pyroclasts and lava samples. Chlorine concentrations in pyroclast matrix glasses are lower than in most melt inclusions. Lava samples with <75 % microlites (<77 wt.% SiO_2) have Cl in a similar range to melt inclusions, and greater than in pyroclast matrix glasses, whereas lava samples with >75 % microlites have dramatically lower Cl concentrations. Fluorine in pyroclast glasses and melt inclusions overlap. Matrix glasses in lava samples with <75 % microlites are higher in fluorine than melt inclusions and pyroclast glasses and increase with increasing SiO_2. However, fluorine concentrations sharply drop off in lava glasses with >75 % microlites.

3.4 Fumarolic gas compositions

Two fumaroles located on top of the shallow intrusion were investigated (Figures 1 and 2B). Fumarole 1 (FUM01) was higher on the bulge created by the 2011–2012 Cordón Caulle laccolith, and had surface temperature of 420 °C. Fumarole 2 (FUM02) was lower on the laccolith, and was 125 °C.

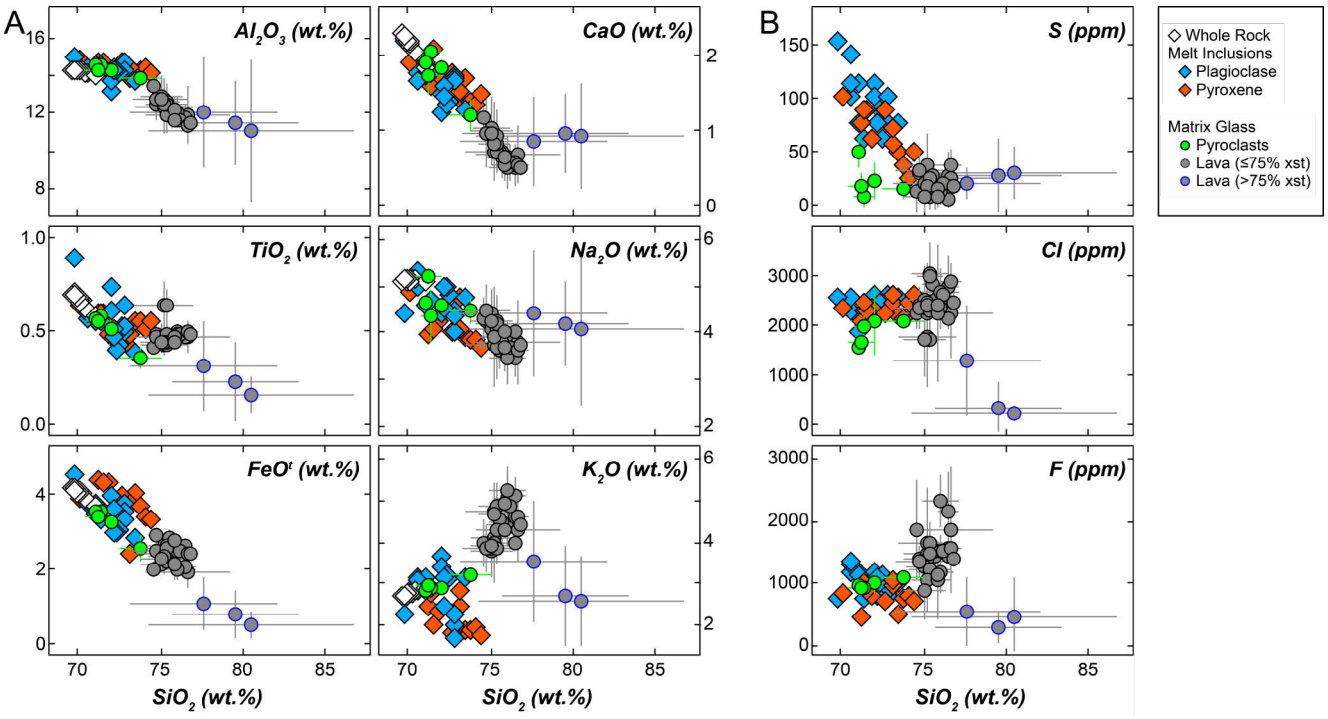

Figure 6: [A] Major elements and [B] volatiles versus SiO_2. Whole-rock and inclusion analyses represent individual points. Matrix glasses are plotted as averages with error bars denoting ± 1 standard deviation. Error bar sizes tend to be larger in more microcrystalline lava samples, indicating higher degrees of intra-sample compositional variability. Major elements are normalised to 100%, volatile-free. All data given in Supplementary Material.

MultiGAS data was only obtained at the 420 °C fumarole (FUM01). High ground temperatures around the fumarole caused anomalous heating of the MultiGAS instrument, causing measurements to become compromised after only a few minutes. Despite this, and the fact that the gas from FUM01 was condensing during the measurement period, sufficient data were obtained to semi-quantitatively assess the composition of the gas being released. The gas was very low in total sulphur and had a strongly hydrothermal signature, with H_2S (maximum 4.7 ppm) far exceeding SO_2 (maximum 0.35 ppm). Molar proportions of H_2O, CO_2, SO_2, H_2S and H_2 recorded by the MultiGAS instrument were 97, 2, 0.003, 0.05 and 0.7 mol%, respectively (Table 1, where data are combined with IC results).

Gas	Molar Ratio (X/H_2S)	Composition (mol %)
H_2O	~2000	97
CO_2	40	2
SO_2	0.06	0.003
H_2S	1	0.05
H_2	14	0.7
HCl	1.6	0.08
HF	1.0	0.05

Table 1 – Gas composition from FUM01 (420 °C). Molar proportions of HCl and HF determined by comparing their ratios to total S in bubblers and MultiGAS

The NaOH bubblers produced solutions with low but measurable chlorine and fluorine at each fumarole. After subtraction of background concentrations in a solution blank (S = 0.226 ppm; Cl = 0.74 ppm; F = 0.20 ppm), the 420 °C fumarole (FUM01) had Cl/F ratio of 2.9 (S = 3.55 ppm; Cl = 6.72 ppm; F = 2.25 ppm), and the 125 °C fumarole (FUM02) had Cl/F ratio of 0.5 (S = 2.07 ppm; Cl = 0.87 ppm; F = 0.45 ppm).

4 Halogen degassing / devolatilisation through each phase of the 2011 Cordón Caulle eruption

4.1 Degassing regimes during explosion, effusion, and intrusion of rhyolite magma

In their classical assessment of Obsidian Dome (Inyo, California), Westrich et al. [1988] described rhyolite degassing as occurring in two regimes. The first is isothermal decompression as magma rises to the surface. This affects all magma involved in the eruption, and includes extensive degassing of pressure-controlled H_2O, CO_2, and S, as well as partitioning of Cl and F into aqueous fluid phases. The second is isobaric crystallisation, as groundmass crystallisation concentrates incompatible volatiles in residual melt and drives "second boiling". This affects only the portions of magma that are emplaced in thermally insulated conditions (flows and intrusions), and includes exsolution of residual H_2O and sulphur, as well as extensive partitioning

of halogens into fluid phases. Westrich et al. [1988] concluded that the shallow intrusive regime was the optimal setting for maximum devolatilisation of rhyolite, because shallow intrusions experience the full effects of both isothermal decompression and isobaric crystallisation, whereas extrusives are too rapidly quenched to allow second boiling, and deep intrusives are at higher pressures where volatiles are more soluble, and may crystallise volatile-bearing phases (e.g. amphiboles, micas, apatite [Westrich et al. 1988], fluorite [Scaillet and Macdonald 2004], or more exotic phases [Elliott 2018]).

4.2 Volatile behaviour during isothermal decompression

Halogen partitioning into aqueous fluids can be modelled under closed- or open-system conditions [Villemant and Boudon 1999; Harford et al. 2003]:

$$\text{Closed}: [X]_f = [X]_i/[(1 - D_X^B)f + D_X^B] \quad (1)$$

$$\text{Open}: [X]_f = [X]_i f^{D_X^B - 1} \quad (2)$$

where $[X]_i$ and $[X]_f$ are initial and final melt concentrations of each volatile species, and $f = 1-(1+k)([H_2O]_i - [H_2O]_f)$ is the fraction of melt remaining after H_2O exsolution and crystallisation of microlites (ς), via the factor $k = (\varsigma/[H_2O]_i - [H_2O]_f)$ and a bulk partition coefficient of $D_X^B = D_X^{v/m}/(1+k)$.

We interpret the two high-sulphur melt inclusions (Figure 6B) to represent the least-degassed Cordón Caulle melts captured by our analyses, and take their average volatile contents as initial values, noting that the low sulphur contents suggest that some degassing had occurred before the inclusions were entrapped. These give $[S]_i$ = 149 ppm, $[Cl]_i$ = 2604 ppm, which are similar to maximum pre-eruptive volatile concentrations previously reported for Cordón Caulle (S ≤160 ppm, Cl ≤2600 ppm by Moune et al. [2012]; S ≤102 ppm, Cl ≤2040 ppm by Castro et al. [2013]), and $[F]_i$ = 1057 ppm, which is higher than previous estimates (F ≤800 ppm by Moune et al. [2012], although they did not specify how they dealt with F-Kα overlaps during EPMA analysis). Because petrological experiments have shown explosively- and effusively-erupted Cordón Caulle magma to have been stored at similar pressure and temperature conditions before eruption [Castro et al. 2013], we consider these initial volatile concentrations to have been equivalent for all magma involved in the eruption.

Textural analysis of the analysed pyroclasts shows no evidence for microlite crystallisation during decompression of the Cordón Caulle magma (Figures 4 and 5A). For post-decompression (but pre-crystallisation) melt volatile contents (denoted $[X]_{f,\Delta P}$) we use the average volatile concentrations in pyroclast glasses: $[S]_{f,\Delta P}$ = 25 ppm, $[Cl]_{f,\Delta P}$ = 1914 ppm, and $[F]_{f,\Delta P}$ = 989 ppm. This is justified for explosive products because volatile contents in pyroclast matrix glasses are similar across all the investigated samples (Figure 6B). We use the same values for effusive and intrusive products because they experienced the same degree of decompression as the pyroclastic melt (albeit at very different decompression rates), and because there is no evidence for uncrystallised matrix glasses in the lava having had volatile contents lower than those in the pyroclasts (Figure 6B).

Water contents were not measured in this work but are necessary for modelling aqueous fluid availability. For $[H_2O]_i$ we use 4 wt.%, the mean measured in suites of melt inclusions from the 2011–2012 eruption [Jay et al. 2014], and consistent with storage at ~4.5 km depth [Newman and Lowenstern 2002; Castro et al. 2013]. For $[H_2O]_f$ we use a single value of 0.1 wt.%, from the narrow and low range of residual H_2O that has consistently been measured in Cordón Caulle eruption products [Schipper et al. 2013; Castro et al. 2014].

Post-decompression chlorine concentrations in matrix glasses ($[Cl]_{f,\Delta P}$) can be explained by closed-system degassing with $D_{Cl}^{v/m}$ of ~10 (Figure 7A). This is within the typical range of $D_{Cl}^{v/m}$ for closed-system degassing of silicic melts [Villemant and Boudon 1999; Villemant et al. 2008; Baker and Alletti 2012] where hydrothermal fluid infiltration is not a factor [Harford et al. 2003]. The modelled $D_{Cl}^{v/m}$ is reasonable and does not require there to have been any Cl-rich salts, brines, or exsolved aqueous fluids in the system at the onset of H_2O degassing. This is despite the fact that Cl-rich brines are stable to high pressure in magmatic systems [Balcone-Boissard et al. 2010]. Even though there was an established hydrothermal system at Cordón Caulle before the eruption, chloride contents of surface waters in this system were low [Sepúlveda et al. 2004]. Furthermore, closed-system degassing as modelled is generally accepted to be the degassing regime that drives explosive volcanic eruptions [Cashman and Sparks 2013].

Post-decompression fluorine concentrations ($[F]_{f,\Delta P}$), if modelled as for chlorine, require $D_F^{v/m}$ to be ~2.5 (Figure 7B). This is significantly higher than the $D_F^{v/m}$<1 that is usually expected in silicic magmas [Baker and Alletti 2012, and references therein], and is noteworthy because any $D_F^{v/m}$>1 implies that fluorine loss via partitioning into aqueous fluids does occur during decompression. The modelled $D_F^{v/m}$ is strongly influenced by our assumptions about the initial concentration of fluorine in the melt. However, our choice of $[F]_i$ is conservative, considering that had we instead used the maximum F (1365 ppm) from our suite of melt inclusions, the modelled $D_F^{v/m}$ would have been >10, for which there is no precedent in silicic melts. The use of maximum F values from a suite of melt inclusions was used in preliminary investigations of the 2011–2012 Cordón Caulle volatile budget [Aguilera et al. 2012a; Moune et al. 2012], but the maxima were lower (800 ppm), and

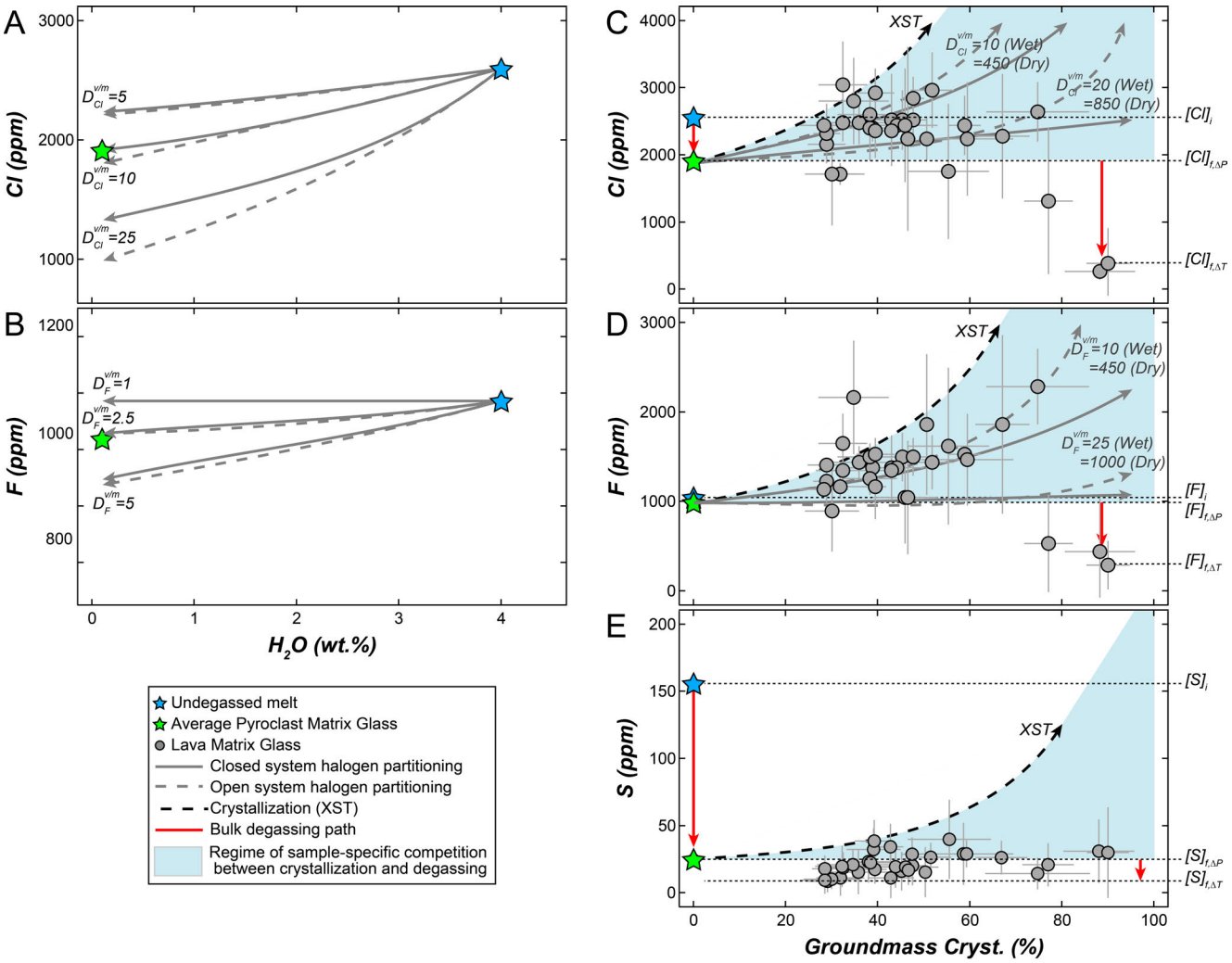

Figure 7: Devolatilisation of Cordón Caulle magma. [A–B] Partitioning of Cl and F into aqueous fluids during isothermal decompression under closed (solid lines) and open (dashed lines) exsolution of H_2O using different $D_X^{v/m}$. Initial H_2O content is from melt inclusion maxima in the literature [Jay et al. 2014], and final H_2O is estimated to be 0.1 wt.% for all magma [Castro et al. 2014]. [C–E] Volatile loss extended to include isobaric crystallisation. Red arrows show magnitude of devolatilisation during decompression and crystallisation. Black dashed arrows show path of volatile incompatibility without being lost from residual melt, and the blue fields mark a region of competition between incompatibility and loss. Models for halogen partitioning during crystallisation are rendered useless by the vast range of aqueous fluid availability that could be assumed. The high-crystallinity lava samples are significantly degassed in Cl and F, and are considered to be representative of most of the flow volume. Sulphur appears to continue to degas, rather than behave incompatibly, across a full range of groundmass crystallinity.

there were no details given on how fluorine EPMA overlaps with other elements were handled in these studies. It may be that fluid-melt partitioning is not the most appropriate mechanism by which to explain fluorine exsolution; but the fact remains that melt inclusions have higher fluorine concentrations than matrix glasses, indicating that exsolution of fluorine was more dramatic than might have been expected (from literature values of $D_F^{v/m}$) during ascent and decompression of the 2011–2012 Cordón Caulle magma. Leachates on fresh ash from the Plinian phase of the eruption have had F ≤167 ppm kg^{-1} of ash [Alloway et al. 2015; Stewart et al. 2016], providing additional evidence for fluorine release during decompression.

4.3 Volatile behaviour during isobaric crystallisation

Halogen behaviour during isobaric crystallisation is often investigated by comparison of Cl and F concentrations to a non-volatile incompatible oxide such as K_2O [Lowenstern et al. 2012]. Here, we instead examine halogen contents as a simple function of groundmass crystallinity (Figure 7C–D), because plagioclase microlites contain a non-trivial orthoclase component so that K_2O is not entirely incompatible during groundmass crystallisation. Also, at high crystallinity (>75 %),

alkali mobility is apparent, with an inflection to decreasing K_2O with increasing SiO_2 Figure 6B). This, as well as inflections in other major elements and halogens, may represent incipient devitrification of the lava matrix at high crystallinity [Lofgren 1970; Stix et al. 1995; Rowe et al. 2012; Schipper et al. 2015]. Qualitatively, most lava samples have halogen concentrations below the maxima that would be expected if chlorine and fluorine behaved entirely incompatibly during isobaric microlite crystallisation (Figure 7C–D, black dashed lines). This becomes more pronounced as crystallinity increases.

The behaviour of the halogens contrasts with that of sulphur (Figure 7E), which significantly degases during decompression but is usually lower in lava samples than pyroclasts, regardless of their degrees of groundmass crystallisation. For modelling the continued degassing of sulphur during isobaric crystallisation, we therefore use $[S]_{f,\Delta T}$ = 9 ppm, which is the detection limit for S by EPMA, and is equivalent to the S measured in many of the lava samples (Figure 7E).

Unfortunately, modelling of halogen partitioning during the crystallisation process (Equations 1 and 2) is rendered virtually meaningless by the requirement for assuming the availability of aqueous fluids in the cooling lava flow. It is evident from the progressive fabric development shown in Figure 4B that porosity and permeability varied immensely in space and time within the flow as it matured. To illustrate the limit of modelling, Figure 7C and 7D illustrate: (1) a "wet" case, where crystallisation proceeds with degassing from the original $[H_2O]_i$ = 4.0 wt.%; and (2) a "dry" case, where fluid is exclusively from second boiling, or $[H_2O]_i$ = 0.1 wt.%. Resulting curves for $D^{v/m}_{X,\text{wet}}$ = 10 fit much of the data reasonably well but are essentially equivalent to the curves for $D^{v/m}_{X,\text{dry}}$ =~450 (Figure 7C–D); a discrepancy too large to be of use.

Notwithstanding this limitation in modelling, the most important feature of the data is that the most extensively crystallised samples from the core of the lava flow are significantly depleted in halogens, not just relative to the maxima expected during crystallisation, but also relative to the post-decompression concentrations ($[X]_{f,\Delta P}$ in Figure 7C–D). This indicates that at high degrees of crystallinity, halogens (as well as alkalis and other elements; Figure 6) become mobile. They achieved final concentrations (denoted $[X]_{f,\Delta T}$ in Figure 7) of $[Cl]_{f,\Delta T}$ = 504 ppm, and $[F]_{f,\Delta T}$ = 385 ppm, and are not significantly retained in the fully evolved and crystallised core of the flow. As noted above, our sample suite contains only three such holocrystalline samples from the flow core, but these are considered to be representative of the majority of the flow (Figure 2A), and the most important to consider in volatile budgets.

We cannot specify whether halogen mobilisation occurs during microlite crystallisation or incipient devitrification (i.e. above or below the glass transition). Indeed, having crystalline SiO_2 (cristobalite) in the groundmass of the most crystalline lava samples indicates that devitrification had begun in the flow core [Figure 4; Damby 2012; Horwell et al. 2013; Schipper et al. 2015], and halogens are known to become mobile (F more so than Cl) during the devitrification of rhyolites [Stix et al. 1995]. The salient point demonstrated by the data is that halogens do mobilise out of the melt during this late-stage evolution in the slowly cooled portions of the lava flow. Appropriate terminology is in question here; with "devolatilisation" being more appropriate than "degassing", as it implies only that the halogens were lost from the melt, but does not specify that they were released in the gas phase [Westrich et al. 1988]. Halogens that did not enter the gas phase may have been transported in aqueous fluids, adsorbed onto glass/mineral surfaces, or formed any number of sublimate crystalline phases that are not accounted for by our analysis [e.g. Delmelle et al. 2007]. To our knowledge, no post-eruptive analyses of such halogen sinks have been made at Cordón Caulle.

The highly crystalline lava core samples are also important for giving some indication as to the state of magma in the syneruptively emplaced laccolith [Castro et al. 2016], which is not exposed at the surface and could not be sampled. Magma in this shallow intrusion is subject to greater thermal insulation and slower cooling rates than even the most central core region of the lava flow. It can therefore be expected to experience the most extensive devolatilisation of any Cordón Caulle magma [Westrich et al. 1988]. The laccolith was emplaced at slightly higher pressure than extruded magma and may have retained enough H_2O to cause its crystallisation sequence to differ slightly from in the flow, but the holocrystalline lava samples are the best available proxy for the textural state of material in the shallow subsurface. Although fluorite stability is strongly pressure-dependent [Scaillet and Macdonald 2004] and other rhyolitic laccoliths have undergone late-stage groundmass crystallisation of fluorine-bearing phases at the nano-scale [e.g. Elliott 2018], it is unclear if such phases would be stable in and around the extremely shallow (~200 metre deep) laccolith at Cordón Caulle. Recent work on exposed rhyolitic laccoliths in Iceland has shown that they have textural characteristics similar to those in the Cordón Caulle flow, including flow banding and a high-density cryptocrystalline groundmass free of any volatile-bearing phases [Mattsson et al. 2018].

5 Total projected sulphur and halogen output from the 2011–2012 Cordón Caulle eruption

We estimate the total output of sulphur (likely to be a minimum due to sulphur degassing prior to melt inclusion entrapment), chlorine and fluorine for each phase

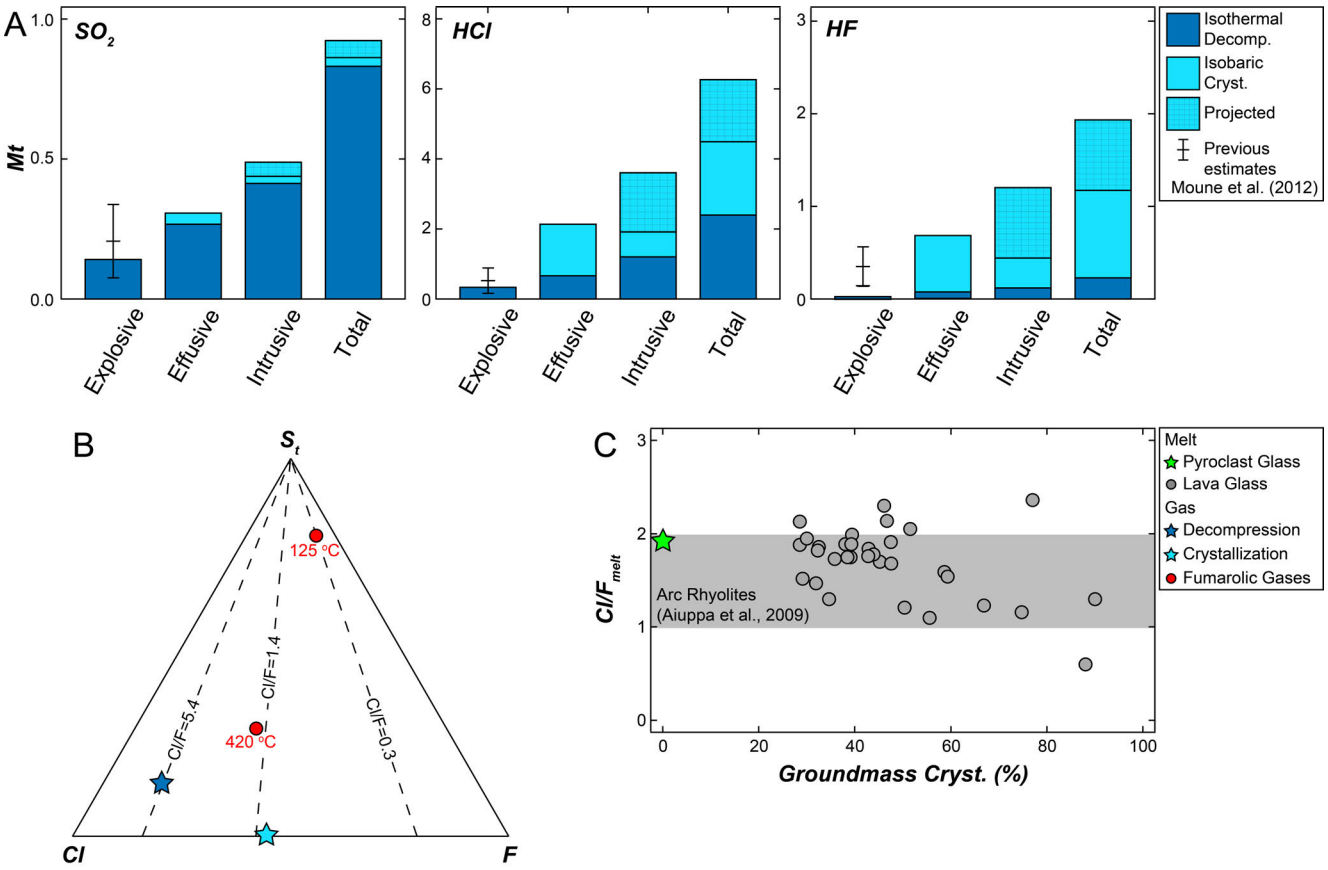

Figure 8: Volatile budget and temporal trends. [A] Histograms of SO_2, HCl, and HF output (in megatons) during different phases of the Cordón Caulle eruption, divided into amounts released during isothermal decompression and to-date and projected amounts from isobaric crystallisation. Previous estimates of volatile output for the opening Plinian phase are from Moune et al. [2012]. [B] Relative molar proportions of S, Cl, and F in gases. Stars represent the petrologically-determined gas compositions for decompression and crystallisation. Note that gas released by isobaric crystallisation has equivalent Cl/F to that measured in the 420 °C fumarole (Cl/F ~1.4), but that both fumaroles have higher-than-predicted proportions of S. [C] Evolution of Cl/F in the melt versus degree of groundmass crystallisation, showing that Cl is lost earlier than F in the crystallisation processes.

of the Cordón Caulle eruption, using a simple mass-balance approach [e.g. Devine et al. 1984; Lowenstern et al. 2012]:

$$G_X = V_m \rho_m \kappa([X]_i - [X]_f) \quad (3)$$

where G_X is the total mass output of each compound, V_m is magma volume, ρ_m is magma density (2500 km^3 based on average whole rock compositions and calculation of Best [2003]), and κ is the ratio of the molecular weights of the volatile compounds to the elemental volatiles. The budgets are expressed in terms of equivalent gaseous volatile compounds (SO_2, HCl, HF), although we recognise that these may not have been the only forms in which the different volatiles were emitted.

We calculate the volatile output during isothermal decompression ± isobaric crystallisation for the magma involved in each phase of the eruption. Decompression is considered to have equally affected all the magma involved in all phases, as it degassed from $[X]_i$ to $[X]_{f,\Delta P}$ (Figure 7C–E). Groundmass crystallisation is considered to have only affected magma in the lava flow and laccolith, as it degassed from $[X]_{f,\Delta P}$ to $[X]_{f,\Delta T}$ (Figure 7C–E).

The total mass of magma erupted as pyroclasts in multiple phases of the Cordón Caulle eruption has been estimated as $6.0 \pm 1.1 \times 10^{11}$ kg [Bonadonna et al. 2015; Pistolesi et al. 2015]. Using this range with $[X]_i$ and $[X]_{f,\Delta P}$ gives total volatile outputs of 0.15 ± 0.03 Mt of SO_2, 0.43 ± 0.07 Mt of HCl, and 0.04 ± 0.01 Mt of HF (Figure 8A). These new values for SO_2 and HCl are within the ranges previously estimated for the Plinian phase of the Cordón Caulle eruption, but our HF estimate is lower by a factor of ~10, seemingly because the fluorine contents we have measured in pyroclast matrix glasses are much higher than those previously reported [163 ppm: Aguilera et al. 2012b; Moune et al. 2012, although analytical details were not given in these abstracts]. The estimated SO_2 output is only slightly lower than satellite-derived estimates of the initial eruptive pulse of SO_2 [0.2 ± 0.04 Mt; Aguilera et al. 2012a; Moune et al. 2012].

For the effusive phase of the eruption, both isother-

mal decompression and isobaric crystallisation must be considered. The total volume of the lava flow has been estimated as 0.45 ± 0.05 km^3 [Tuffen et al. 2013; Farquharson et al. 2015], over an area of ~7.2 km^2. The partially-glassy upper surface and breakouts make up ~15 % of the flow volume (based on upper vitryphyre being ~1 m thick (Figure 2A), and breakout volumes estimated by Magnall et al. [2018]), with an average porosity of 30 vol.%. The crystalline lava core is considered to be avesicular. The estimated total dense rock equivalent (DRE) volume of the entire lava flow is therefore 0.43 ± 0.05 km^3, and of its crystalline core is 0.39 ± 0.04 km^3. The total output from the lava flow through decompression (all lava) and by crystallisation (core only) is therefore calculated to be 0.30 ± 0.03 Mt of SO_2, 2.18 ± 0.23 Mt of HCl, and 0.70 ± 0.07 Mt of HF (Figure 8A).

The shallow intrusive environment should be the zone of maximum devolatilisation [Westrich et al. 1988], and the Cordón Caulle laccolith therefore contributes substantially to the volatile budget of the eruption. The laccolith would have experienced both isothermal decompression ($[X]_i$ to $[X]_{f,\Delta P}$) and isobaric crystallisation ($[X]_{f,\Delta P}$ to $[X]_{f,\Delta T}$; Figure 7C–E), and has an estimated volume of 0.8 km^3 [Castro et al. 2016]. A porosity range similar to the lava (0–30 vol.%) allows bracketing of the DRE magma volumes in degassing calculations, and this is highly conservative given the negligible porosity of the holocrystalline lava samples (Figure 4) and rhyolitic laccoliths elsewhere [Mattsson et al. 2018]. The total potential volatile output from decompression and crystallisation of the laccolith is therefore 0.48 ± 0.08 Mt of SO_2, 3.67 ± 0.65 Mt of HCl, and 1.20 ± 0.21 Mt of HF (Figure 8A).

Overall, the total projected volatile output from all phases of the 2011–2012 eruption is 0.92 Mt of SO_2, 6.27 Mt of HCl, and 1.94 Mt of HF. Here, it is noteworthy that the effusive and intrusive phases contribute overwhelmingly to the total volatile output, with the opening explosive phase contributing only 16 wt.% of total SO_2, 7 wt.% of total HCl and 2 wt.% of total HF. The total SO_2 output (0.92 Mt) initially appears high, given the low satellite-derived SO_2 output from the 2011 Plinian phase [0.2 ± 0.04 Mt; Aguilera et al. 2012a; Moune et al. 2012] and the low concentrations of total sulphur in the 420 °C fumarole measured in 2017 (Table 1). However, as seen in Figure 8A, the vast majority of SO_2 output is attributed to decompression of the magma that formed the lava flow and laccolith, during an extended eruptive period over which there were no gas measurements made. The satellite-derived estimates only account for decompression during the opening Plinian phase and fumarolic measurements only account for the subsequent isobaric crystallisation process; therefore, the majority of SO_2 output would have gone unmeasured.

6 Long-term rhyolite devolatilisation

Numeric models show that the cooling of thick rhyolite lavas and intrusions takes decades to centuries [Manley 1992; Mattsson et al. 2018], and the Cordón Caulle laccolith should therefore be far from fully crystalline at the time of writing (~7.5 years after the eruption). The volatile budgets given above represent potential output, to be eventually realised. Volatile output to-date includes the full decompressive complement, but only a fraction of the potential output from isobaric crystallisation, which is corroborated by the dominantly hydrothermal but halogen-bearing fumarolic gas emissions. In Figure 8A we illustrate the discrepancy between to-date and eventual emissions with the crude assumption that ~70 % of the laccolith could still be in a molten state. This predicts that the gas currently being emitted from the cooling laccolith should be low in sulphur, and comparatively rich in halogens.

In Figure 8B, we compare the relative S, Cl, and F concentrations in gases predicted by our petrologic models for isothermal decompression and isobaric crystallisation, to those measured at fumaroles in 2017. The petrologic models predict crystallisation to release gas that is lower in sulphur, and has higher Cl/F than the gas released during decompression. The gas from the 420 °C fumarole has Cl/F that is nearly identical to that predicted for isobaric crystallisation; however, both fumaroles have proportionally higher concentrations of sulphur than the petrologic models would predict. This "excess sulphur" from the fumaroles, although of very limited magnitude (e.g. low total sulphur concentrations from the 420 °C fumarole: Table 1), may be the result of degassing from other post-eruptive (i.e. not the laccolith) intrusions into the Cordón Caulle edifice, the deformation from which has been documented [Delgado et al. 2016].

As crystallisation progresses, Cl deviates from incompatible behaviour and partitions out of the melt earlier than F (Figure 7C–D). This is reflected in Cl/F ratios in residual melt decreasing with increasing crystallisation, although the Cordón Caulle matrix glasses mostly remain within the typical range of Cl/F for arc rhyolites (Figure 8C; Aiuppa et al. [2009]), and is further reflected in the 125 °C fumarole having lower Cl/F than the 420 °C fumarole (Figure 8B). There are few published data on Cl/F in gases from arc rhyolites [Pyle and Mather 2009], but the Cl/F ratios in Cordón Caulle gases are similar to those emitted from fumaroles in the rhyolite system at Satsuma-Iwojima [Japan: Shinohara et al. 1993; Mori et al. 2002]. Our Cordón Caulle gas data are too sparse to draw any strong conclusions, but they corroborate early dominance of Cl over F in emitted gases, with F becoming dominant at high degrees of cooling and crystallisation.

7 Conclusions

The degassing—or devolatilisation—of chlorine and fluorine from silicic magmas can have severe impacts on the surrounding environment [Cronin et al. 2003; Bellomo et al. 2007], and fluorosis following the 2011–2012 Cordón Caulle eruption has adversely affected livestock and wild deer populations in South America [Flueck and Smith-Flueck 2013; Stewart et al. 2016]. Our petrological approach to sulphur and halogen mobilisation during the eruption highlights that while sulphur dominantly degases during magma decompression, halogen release is most dramatic from thermally insulated, effusive and/or intrusive rhyolites. This needs to be taken into consideration when evaluating volatile budgets and long-term impacts of large eruptions.

The 2011–2012 eruption of Cordón Caulle is the largest eruption to-date of the 21st century, and halogen release from the magma involved in this eruption is far from complete. Fumaroles atop the cooling laccolith and hydrothermal fluids circulating through the edifice will likely continue to become progressively more fluorine-rich with time.

Acknowledgements

CIS acknowledges funding from Victoria University of Wellington, and subcontract to BMK's Ministry of Business and Innovation Catalyst fund. BMK and GS acknowledge the Marsden fund.

Author contributions

CIS participated in all fieldwork, performed EPMA analyses, and wrote the paper. JMC and BMK co-led fieldwork, and JMC performed XRD analyses. BWC provided bubblers and performed IC measurements. AA provided the MultiGAS instrument and processed its data. BA, PF and GS enabled fieldwork in 2017. HT co-led many of the field expeditions. All authors contributed to interpretation of the data.

Data availability

All data are available in supplementary materials.

References

Aguilera, F., F. Gutierrez, S. Moune, S. Carn, P. Sánchez, C. Bucarey, C. Tambley, and J. Bastıas (2012a). "Volatile budget of the 2011 Cordón Caulle eruption, Southern Volcanic Zone, Chile". *XIII Congreso Geológico Chileno, August*. Vol. 5.

Aguilera, F., F. Tassi, T. Darrah, S. Moune, and O. Vaselli (2012b). "Geochemical model of a magmatic–hydrothermal system at the Lastarria volcano, northern Chile". *Bulletin of Volcanology* 74.1, pp. 119–134. DOI: 10.1007/s00445-011-0489-5.

Aiuppa, A. (2005). "Chemical mapping of a fumarolic field: La Fossa Crater, Vulcano Island (Aeolian Islands, Italy)". *Geophysical Research Letters* 32.13. DOI: 10.1029/2005gl023207.

Aiuppa, A., D. Baker, and J. Webster (2009). "Halogens in volcanic systems". *Chemical Geology* 263.1-4, pp. 1–18. DOI: 10.1016/j.chemgeo.2008.10.005.

Alloway, B. V., N. J. G. Pearce, G. Villarosa, V. Outes, and P. I. Moreno (2015). "Multiple melt bodies fed the AD 2011 eruption of Puyehue-Cordón Caulle, Chile". *Scientific Reports* 5.1. DOI: 10.1038/srep17589.

Baker, D. R. and M. Alletti (2012). "Fluid saturation and volatile partitioning between melts and hydrous fluids in crustal magmatic systems: The contribution of experimental measurements and solubility models". *Earth-Science Reviews* 114.3-4, pp. 298–324. DOI: 10.1016/j.earscirev.2012.06.005.

Baker, D. R. and H. Balcone-Boissard (2009). "Halogen diffusion in magmatic systems: Our current state of knowledge". *Chemical Geology* 263.1-4, pp. 82–88. DOI: 10.1016/j.chemgeo.2008.10.010.

Balcone-Boissard, H., B. Villemant, and G. Boudon (2010). "Behavior of halogens during the degassing of felsic magmas". *Geochemistry Geophysics Geosystems* 11.9. DOI: 10.1029/2010gc003028.

Bégué, F., C. D. Deering, D. M. Gravley, I. Chambefort, and B. M. Kennedy (2017). "From source to surface: Tracking magmatic boron and chlorine input into the geothermal systems of the Taupo Volcanic Zone, New Zealand". *Journal of Volcanology and Geothermal Research* 346, pp. 141–150. DOI: 10.1016/j.jvolgeores.2017.03.008.

Bellomo, S., A. Aiuppa, W. D'Alessandro, and F. Parello (2007). "Environmental impact of magmatic fluorine emission in the Mt. Etna area". *Journal of Volcanology and Geothermal Research* 165.1-2, pp. 87–101. DOI: 10.1016/j.jvolgeores.2007.04.013.

Best, M. G. (2003). *Igneous and metamorphic petrology*. 2nd ed. John Wiley & Sons.

Bonadonna, C., M. Pistolesi, R. Cioni, W. Degruyter, M. Elissondo, and V. Baumann (2015). "Dynamics of wind-affected volcanic plumes: The example of the 2011 Cordón Caulle eruption, Chile". *Journal of Geophysical Research: Solid Earth* 120.4, pp. 2242–2261. DOI: 10.1002/2014jb011478.

Carroll, M. R. (1994). "Solubilities of sulfur, noble gases, nitrogen, chlorine, and fluorine in magmas". *Reviews in Mineralogy and Geochemistry* 30, pp. 87–101.

Cashman, K. V. and R. S. J. Sparks (2013). "How volcanoes work: A 25 year perspective". *Geological Society of America Bulletin* 125.5-6, pp. 664–690. doi: 10.1130/b30720.1.

Cashman, K. V. (2004). "Volatile controls on magma ascent and eruption". *The State of the Planet: Frontiers and Challenges in Geophysics, Volume 150*. Ed. by R. Sparks and C. Hawkesworth. American Geophysical Union, pp. 109–124. doi: 10.1029/150gm10.

Castro, J. M., I. N. Bindeman, H. Tuffen, and C. I. Schipper (2014). "Explosive origin of silicic lava: Textural andδD–H 2 O evidence for pyroclastic degassing during rhyolite effusion". *Earth and Planetary Science Letters* 405, pp. 52–61. doi: 10.1016/j.epsl.2014.08.012.

Castro, J. M., B. Cordonnier, C. I. Schipper, H. Tuffen, T. S. Baumann, and Y. Feisel (2016). "Rapid laccolith intrusion driven by explosive volcanic eruption". *Nature Communications* 7.1. doi: 10.1038/ncomms13585.

Castro, J. M., C. I. Schipper, S. P. Mueller, A. S. Militzer, A. Amigo, C. S. Parejas, and D. Jacob (2013). "Storage and eruption of near-liquidus rhyolite magma at Cordón Caulle, Chile". *Bulletin of Volcanology* 75.4. doi: 10.1007/s00445-013-0702-9.

Cronin, S. J., V. Neall, J. Lecointre, M. Hedley, and P. Loganathan (2003). "Environmental hazards of fluoride in volcanic ash: a case study from Ruapehu volcano, New Zealand". *Journal of Volcanology and Geothermal Research* 121.3-4, pp. 271–291. doi: 10.1016/s0377-0273(02)00465-1.

D'Alessandro, W. (2006). "Human fluorosis related to volcanic activity: a review". *Environmental Toxicology*. WIT Press. doi: 10.2495/etox060031.

Damby, D. (2012). "From dome to disease: The respiratory toxicity of volcanic cristobalite". PhD thesis. Durham University.

de Hoog, J. C. M., M. J. van Bergen, and M. H. G. Jacobs (2005). "Vapour-phase crystallisation of silica from SiF_4-bearing volcanic gases". *Annals of Geophysics* 48.4-5. issn: 2037-416X. doi: 10.4401/ag-3233.

Deer, W., R. Howie, and J. Zussman (1992). *An introduction to the rock-forming minerals*. 2nd ed. New York: John Wiley and Sons.

Delgado, F., M. E. Pritchard, D. Basualto, J. Lazo, L. Córdova, and L. E. Lara (2016). "Rapid reinflation following the 2011-2012 rhyodacite eruption at Cordón Caulle volcano (Southern Andes) imaged by InSAR: Evidence for magma reservoir refill". *Geophysical Research Letters* 43.18, pp. 9552–9562. doi: 10.1002/2016gl070066.

Delmelle, P. (2003). "Environmental impacts of tropospheric volcanic gas plumes". *Geological Society, London, Special Publications* 213.1, pp. 381–399. doi: 10.1144/gsl.sp.2003.213.01.23.

Delmelle, P., M. Lambert, Y. Dufrêne, P. Gerin, and N. Óskarsson (2007). "Gas/aerosol–ash interaction in volcanic plumes: New insights from surface analyses of fine ash particles". *Earth and Planetary Science Letters* 259.1-2, pp. 159–170. doi: 10.1016/j.epsl.2007.04.052.

Devine, J. D., H. Sigurdsson, A. N. Davis, and S. Self (1984). "Estimates of sulfur and chlorine yield to the atmosphere from volcanic eruptions and potential climatic effects". *Journal of Geophysical Research: Solid Earth* 89.B7, pp. 6309–6325. doi: 10.1029/jb089ib07p06309.

Dingwell, D. B. and K. U. Hess (1998). "Melt viscosities in the system Na-Fe-Si-O-F-Cl; contrasting effects of F and Cl in alkaline melts". *American Mineralogist* 83.9-10, pp. 1016–1021. doi: 10.2138/am-1998-9-1009.

Edmonds, M., D. Pyle, and C. Oppenheimer (2002). "HCl emissions at Soufrière Hills Volcano, Montserrat, West Indies, during a second phase of dome building: November 1999 to October 2000". *Bulletin of Volcanology* 64.1, pp. 21–30. doi: 10.1007/s00445-001-0175-0.

Edmonds, M. and P. J. Wallace (2017). "Volatiles and Exsolved Vapor in Volcanic Systems". *Elements* 13.1, pp. 29–34. doi: 10.2113/gselements.13.1.29.

Elliott, B. (2018). "Petrogenesis of Heavy Rare Earth Element Enriched Rhyolite: Source and Magmatic Evolution of the Round Top Laccolith, Trans-Pecos, Texas". *Minerals* 8.10, p. 423. doi: 10.3390/min8100423.

Farquharson, J., M. James, and H. Tuffen (2015). "Examining rhyolite lava flow dynamics through photo-based 3D reconstructions of the 2011–2012 lava flowfield at Cordón-Caulle, Chile". *Journal of Volcanology and Geothermal Research* 304, pp. 336–348. doi: 10.1016/j.jvolgeores.2015.09.004.

Flueck, W. T. and J. A. M. Smith-Flueck (2013). "Severe dental fluorosis in juvenile deer linked to a recent volcanic eruption in Patagonia". *Journal of Wildlife Diseases* 49.2, pp. 355–366. doi: 10.7589/2012-11-272.

Gerlach, D. C., F. A. Frey, H. Moreno-Roa, and L. Lopez-Escobar (1988). "Recent volcanism in the Puyehue—Cordon Caulle region, Southern Andes, Chile (40· 5° S): petrogenesis of evolved lavas". *Journal of Petrology* 29.2, pp. 333–382. doi: 10.1093/petrology/29.2.333.

Giggenbach, W. F. (1996). "Chemical Composition of Volcanic Gases". *Monitoring and Mitigation of Volcano Hazards*. Ed. by R. Scarpa and R. Tilling. Springer Berlin Heidelberg, pp. 221–256. doi: 10.1007/978-3-642-80087-0_7.

Gualda, G. A. R. and M. S. Ghiorso (2013). "Low-Pressure Origin of High-Silica Rhyolites and Granites". *The Journal of Geology* 121.5, pp. 537–545. doi: 10.1086/671395.

Harford, C., R. Sparks, and A. Fallick (2003). "Degassing at the Soufriere Hills Volcano, Montserrat, Recorded in Matrix Glass Compositions". *Journal of Petrology* 44.8, pp. 1503–1523. DOI: 10.1093/petrology/44.8.1503.

Horwell, C. J., B. J. Williamson, E. W. Llewellin, D. E. Damby, and J. S. L. Blond (2013). "The nature and formation of cristobalite at the Soufrière Hills volcano, Montserrat: implications for the petrology and stability of silicic lava domes". *Bulletin of Volcanology* 75.3. DOI: 10.1007/s00445-013-0696-3.

Jarosewich, E., J. Nelen, and J. A. Norberg (1980). "Reference Samples for Electron Microprobe Analysis". *Geostandards and Geoanalytical Research* 4.1, pp. 43–47. DOI: 10.1111/j.1751-908x.1980.tb00273.x.

Jay, J., F. Costa, M. Pritchard, L. Lara, B. Singer, and J. Herrin (2014). "Locating magma reservoirs using InSAR and petrology before and during the 2011–2012 Cordón Caulle silicic eruption". *Earth and Planetary Science Letters* 395, pp. 254–266. DOI: 10.1016/j.eps1.2014.03.046.

Jochum, K. P., U. Nohl, K. Herwig, E. Lammel, B. Stoll, and A. W. Hofmann (2005). "GeoReM: A New Geochemical Database for Reference Materials and Isotopic Standards". *Geostandards and Geoanalytical Research* 29.3, pp. 333–338. DOI: 10.1111/j.1751-908x.2005.tb00904.x.

Kilinc, I. A. and C. W. Burnham (1972). "Partitioning of Chloride Between a Silicate Melt and Coexisting Aqueous Phase from 2 to 8 Kilobars". *Economic Geology* 67.2, pp. 231–235. DOI: 10.2113/gsecongeo.67.2.231.

Lara, L., H. Moreno, J. Naranjo, S. Matthews, and C. P. de Arce (2006). "Magmatic evolution of the Puyehue–Cordón Caulle Volcanic Complex (40° S), Southern Andean Volcanic Zone: From shield to unusual rhyolitic fissure volcanism". *Journal of Volcanology and Geothermal Research* 157.4, pp. 343–366. DOI: 10.1016/j.jvolgeores.2006.04.010.

Lofgren, G. (1970). "Experimental Devitrification Rate of Rhyolite Glass". *GSA Bulletin* 81.2, pp. 553–560. ISSN: 0016-7606. DOI: 10.1130/0016-7606(1970)81[553:EDRORG]2.0.CO;2. eprint: https://pubs.geoscienceworld.org/gsabulletin/article-pdf/81/2/553/3428481/i0016-7606-81-2-553.pdf.

Lowenstern, J. B., H. Bleick, J. A. Vazquez, J. M. Castro, and P. B. Larson (2012). "Degassing of Cl, F, Li, and Be during extrusion and crystallization of the rhyolite dome at Volcán Chaitén, Chile during 2008 and 2009". *Bulletin of Volcanology* 74.10, pp. 2303–2319. DOI: 10.1007/s00445-012-0663-4.

Magnall, N., M. R. James, H. Tuffen, and C. Vye-Brown (2017). "Emplacing a Cooling-Limited Rhyolite Lava Flow: Similarities with Basaltic Lava Flows". *Frontiers in Earth Science* 5. DOI: 10.3389/feart.2017.00044.

Magnall, N., M. R. James, H. Tuffen, C. Vye-Brown, C. I. Schipper, J. M. Castro, and A. G. Davies (2018). "The origin and evolution of breakouts in a cooling-limited rhyolite lava flow". *GSA Bulletin* 131.1-2, pp. 137–154. DOI: 10.1130/b31931.1.

Manley, C. R. (1992). "Extended cooling and viscous flow of large, hot rhyolite lavas: implications of numerical modeling results". *Journal of Volcanology and Geothermal Research* 53.1-4, pp. 27–46. DOI: 10.1016/0377-0273(92)90072-1.

Mattsson, T., S. Burchardt, B. S. G. Almqvist, and E. Ronchin (2018). "Syn-Emplacement Fracturing in the Sandfell Laccolith, Eastern Iceland—Implications for Rhyolite Intrusion Growth and Volcanic Hazards". *Frontiers in Earth Science* 6. DOI: 10.3389/feart.2018.00005.

McPhie, J., V. Kamenetsky, S. Allen, K. Ehrig, A. Agangi, and A. Bath (2011). "The fluorine link between a supergiant ore deposit and a silicic large igneous province". *Geology* 39.11, pp. 1003–1006. DOI: 10.1130/g32205.1.

Metrich, N. and M. Rutherford (1992). "Experimental study of chlorine behavior in hydrous silicic melts". *Geochimica et Cosmochimica Acta* 56.2, pp. 607–616. DOI: 10.1016/0016-7037(92)90085-w.

Mori, T., M. Sato, Y. Shimoike, and K. Notsu (2002). "High SiF4/HF ratio detected in Satsuma-Iwojima volcano's plume by remote FT-IR observation". *Earth, Planets and Space* 54.3, pp. 249–256. DOI: 10.1186/bf03353024.

Moune, S., S. Carn, N. Cluzel, F. Aguilera, and A. Amigo (2012). "Volatile Budget of the 2011 Cordon Caulle Eruption (Chile) from Various and Integrated Approaches." Vol. 76. 6, p. 2140. eprint: https://pubs.geoscienceworld.org/minmag/article-pdf/76/6/2045/2920060/gsminmag.76.6.13-M.pdf.

Newman, S. and J. B. Lowenstern (2002). "VolatileCalc: a silicate melt–H2O–CO2 solution model written in Visual Basic for excel". *Computers & Geosciences* 28.5, pp. 597–604. DOI: 10.1016/s0098-3004(01)00081-4.

Pistolesi, M., R. Cioni, C. Bonadonna, M. Elissondo, V. Baumann, A. Bertagnini, L. Chiari, R. Gonzales, M. Rosi, and L. Francalanci (2015). "Complex dynamics of small-moderate volcanic events: the example of the 2011 rhyolitic Cordón Caulle eruption, Chile". *Bulletin of Volcanology* 77.1. DOI: 10.1007/s00445-014-0898-3.

Pyle, D. and T. Mather (2009). "Halogens in igneous processes and their fluxes to the atmosphere and oceans from volcanic activity: A review". *Chemical Geology* 263.1-4, pp. 110–121. DOI: 10.1016/j.chemgeo.2008.11.013.

Roberts, T. J. et al. (2017). "Validation of a novel Multi-Gas sensor for volcanic HCl alongside H_2S and SO_2 at Mt. Etna". *Bulletin of Volcanology* 79.5. DOI: 10.1007/s00445-017-1114-z.

Rowe, M. C., B. S. Ellis, and A. Lindeberg (2012). "Quantifying crystallization and devitrification of rhyolites by means of X-ray diffraction and electron microprobe analysis". *American Mineralogist* 97.10, pp. 1685–1699. doi: 10.2138/am.2012.4006.

Scaillet, B. and R. Macdonald (2004). "Fluorite stability in silicic magmas". *Contributions to Mineralogy and Petrology* 147.3, pp. 319–329. doi: 10.1007/s00410-004-0559-1.

Schipper, C. I., J. M. Castro, H. Tuffen, M. R. James, and P. How (2013). "Shallow vent architecture during hybrid explosive–effusive activity at Cordón Caulle (Chile, 2011–12): Evidence from direct observations and pyroclast textures". *Journal of Volcanology and Geothermal Research* 262, pp. 25–37. doi: 10.1016/j.jvolgeores.2013.06.005.

Schipper, C. I., J. M. Castro, H. Tuffen, F. B. Wadsworth, D. Chappell, A. E. Pantoja, M. P. Simpson, and E. C. L. Ru (2015). "Cristobalite in the 2011–2012 Cordón Caulle eruption (Chile)". *Bulletin of Volcanology* 77.5. doi: 10.1007/s00445-015-0925-z.

Schipper, C. I., C. Mandon, A. Maksimenko, J. M. Castro, C. E. Conway, P. Hauer, M. Kirilova, and G. Kilgour (2017). "Vapor-phase cristobalite as a durable indicator of magmatic pore structure and halogen degassing: an example from White Island volcano (New Zealand)". *Bulletin of Volcanology* 79.10. doi: 10.1007/s00445-017-1157-1.

Schneider, C. A., W. S. Rasband, and K. W. Eliceiri (2012). "NIH Image to ImageJ: 25 years of image analysis". *Nature Methods* 9.7, pp. 671–675. doi: 10.1038/nmeth.2089.

Sepúlveda, F., K. Dorsch, A. Lahsen, S. Bender, and C. Palacios (2004). "Chemical and isotopic composition of geothermal discharges from the Puyehue-Cordón Caulle area (40.5°S), Southern Chile". *Geothermics* 33.5, pp. 655–673. doi: 10.1016/j.geothermics.2003.10.005.

Shinohara, H. (2005). "A new technique to estimate volcanic gas composition: plume measurements with a portable multi-sensor system". *Journal of Volcanology and Geothermal Research* 143.4, pp. 319–333. doi: 10.1016/j.jvolgeores.2004.12.004.

Shinohara, H., W. F. Giggenbach, K. Kazahaya, and J. W. Hedenquist (1993). "Geochemistry of volcanic gases and hot springs of Satsuma-Iwojima, Japan: Following Matsuo." *Geochemical Journal* 27.4/5, pp. 271–285. doi: 10.2343/geochemj.27.271.

Singer, B. S., B. R. Jicha, M. A. Harper, J. A. Naranjo, L. E. Lara, and H. Moreno-Roa (2008). "Eruptive history, geochronology, and magmatic evolution of the Puyehue-Cordon Caulle volcanic complex, Chile". *Geological Society of America Bulletin* 120.5-6, pp. 599–618. doi: 10.1130/b26276.1.

Sparks, R. S. J. (2003). "Dynamics of magma degassing". *Geological Society, London, Special Publications* 213.1, pp. 5–22. doi: 10.1144/gsl.sp.2003.213.01.02.

Stewart, C., H. M. Craig, S. Gaw, T. Wilson, G. Villarosa, V. Outes, S. Cronin, and C. Oze (2016). "Fate and agricultural consequences of leachable elements added to the environment from the 2011 Cordón Caulle tephra fall". *Journal of Volcanology and Geothermal Research* 327, pp. 554–570. doi: 10.1016/j.jvolgeores.2016.09.017.

Stix, J., G. D. Layne, and T. L. Spell (1995). "The behavior of light lithophile and halogen elements in felsic magma: geochemistry of the post-caldera Valles Rhyolites, Jemez Mountains Volcanic Field, New Mexico". *Journal of Volcanology and Geothermal Research* 67.1-3, pp. 61–77. doi: 10.1016/0377-0273(94)00098-2.

Symonds, R., T. Gerlach, and M. Reed (2001). "Magmatic gas scrubbing: implications for volcano monitoring". *Journal of Volcanology and Geothermal Research* 108.1-4, pp. 303–341. doi: 10.1016/s0377-0273(00)00292-4.

Symonds, R. B., W. I. Rose, M. H. Reed, F. E. Lichte, and D. L. Finnegan (1987). "Volatilization, transport and sublimation of metallic and non-metallic elements in high temperature gases at Merapi Volcano, Indonesia". *Geochimica et Cosmochimica Acta* 51.8, pp. 2083–2101. doi: 10.1016/0016-7037(87)90258-4.

Tuffen, H., M. R. James, J. M. Castro, and C. I. Schipper (2013). "Exceptional mobility of an advancing rhyolitic obsidian flow at Cordón Caulle volcano in Chile". *Nature Communications* 4.1. doi: 10.1038/ncomms3709.

Villemant, B. and G. Boudon (1999). "H_2O and halogen (F, Cl, Br) behaviour during shallow magma degassing processes". *Earth and Planetary Science Letters* 168.3-4, pp. 271–286. doi: 10.1016/s0012-821x(99)00058-8.

Villemant, B., J. Mouatt, and A. Michel (2008). "Andesitic magma degassing investigated through H2O vapour–melt partitioning of halogens at Soufrière Hills Volcano, Montserrat (Lesser Antilles)". *Earth and Planetary Science Letters* 269.1-2, pp. 212–229. doi: 10.1016/j.eps1.2008.02.014.

von Glasow, R., N. Bobrowski, and C. Kern (2009). "The effects of volcanic eruptions on atmospheric chemistry". *Chemical Geology* 263.1-4, pp. 131–142. doi: 10.1016/j.chemgeo.2008.08.020.

Wardell, L., P. Kyle, and D. Counce (2008). "Volcanic emissions of metals and halogens from White Island (New Zealand) and Erebus volcano (Antarctica) determined with chemical traps". *Journal of Volcanology and Geothermal Research* 177.3, pp. 734–742. doi: 10.1016/j.jvolgeores.2007.07.007.

Waters, J. et al. (2006). "The Earth observing system microwave limb sounder (EOS MLS) on the aura Satellite". *IEEE Transactions on Geoscience and Remote Sensing* 44.5, pp. 1075–1092. doi: 10.1109/tgrs.2006.873771.

Webster, J. D. (1990). "Partitioning of F between H2O and CO2 fluids and topaz rhyolite melt". *Contribu-*

tions to Mineralogy and Petrology 104.4, pp. 424–438. DOI: 10.1007/bf01575620.

Webster, J. D., D. R. Baker, and A. Aiuppa (2018). "Halogens in Mafic and Intermediate-Silica Content Magmas". *Springer Geochemistry*. Ed. by H. D. and A. L. Springer International Publishing, pp. 307–430. DOI: 10.1007/978-3-319-61667-4_6.

Westrich, H. R., H. W. Stockman, and J. C. Eichelberger (1988). "Degassing of rhyolitic magma during ascent and emplacement". *Journal of Geophysical Research* 93.B6, p. 6503. DOI: 10.1029/jb093ib06p06503.

Witter, J. B. and S. M. Kuehner (2004). "A simple empirical method for high-quality electron microprobe analysis of fluorine at trace levels in Fe-bearing minerals and glasses". *American Mineralogist* 89.1, pp. 57–63. DOI: 10.2138/am-2004-0108.

Wolff-Boenisch, D., S. R. Gislason, and E. H. Oelkers (2004). "The effect of fluoride on the dissolution rates of natural glasses at pH 4 and 25°C". *Geochimica et Cosmochimica Acta* 68.22, pp. 4571–4582. DOI: 10.1016/j.gca.2004.05.026.

Zhang, C., J. Koepke, L.-X. Wang, P. E. Wolff, S. Wilke, A. Stechern, R. Almeev, and F. Holtz (2016). "A Practical Method for Accurate Measurement of Trace Level Fluorine in Mg- and Fe-Bearing Minerals and Glasses Using Electron Probe Microanalysis". *Geostandards and Geoanalytical Research* 40.3, pp. 351–363. DOI: 10.1111/j.1751-908x.2015.00390.x.